Research Square

Preprints are preliminary reports that have not undergone peer review.
They should not be considered conclusive, used to inform clinical practice,
or referenced by the media as validated information.

Study on Rapid Support Technology for Deep Large-Inclination Hard Rock Roadway

Kexin Bai

baikexin854@163.com

Shunhe Coal Mine,Yongcheng Coal Industry Group Co. ,Ltd

Article

Keywords: deep mining, large-inclination roadway, roadway support

Posted Date: November 23rd, 2026

DOI: https://doi.org/10.21203/rs.3.rs-11588571/v1

License: This work is licensed under a Creative Commons Attribution 4.0 International License.
Read Full License

Additional Declarations: No competing interests reported.

Study on Rapid Support Technology for Deep Large-Inclination Hard Rock Roadway

Bai Kexing

Shunhe Coal Mine,Yongcheng Coal Industry Group Co. ,Ltd.

Corresponding author: Kexin Bai; E-mail: baikexin854@163.com

Abstract: To address the complex conditions of large burial depth, hard lithology, and steep inclination in the return air inclined blind shaft (lower section) of Shunhe Coal Mine, a systematic study was conducted through field monitoring, theoretical analysis, rock physical and mechanical property tests, and FLAC³D numerical simulation. The evolution laws of surrounding rock deformation, stress distribution, and plastic zone under different inclination angles were investigated, revealing the influence mechanism of inclination angle on surrounding rock stability, which provides a theoretical basis for support parameter optimization. On this basis, the permanent support parameters were optimized: the bolt spacing was enlarged to 1000 mm × 1000 mm, the anchor cables were upgraded to 1×19-strand high-strength low-relaxation steel strands with spacing adjusted to 1300 mm × 2000 mm. The drilling workload for support after optimization was reduced by 23.3% compared with the original scheme. Numerical simulation verification indicates that the optimized scheme can effectively control the expansion of the plastic zone and roadway deformation, significantly reducing the support operation intensity while ensuring surrounding rock stability, thus creating favorable conditions for rapid excavation in deep large-inclination roadways. The research results can provide a reference for rapid support design and construction in roadways under similar complex conditions.

Keywords: deep mining; large-inclination roadway; roadway support

1 Introduction

Deep roadway excavation under high in situ stress can trigger progressive fracturing and deformation, increasing the demands on permanent support [1–3]. Stress magnitude, principal stress orientation, and excavation unloading jointly influence surrounding rock stability [4,5]. For deep inclined hard rock roadways, support design must therefore balance deformation control with the drilling and installation workload within each excavation cycle.

Studies of principal stress rotation and inclined stratification associate asymmetric deformation with stress direction, structural interfaces, and roadway geometry [6,7]. Investigations of steeply dipping seams, true triaxial experiments, and analyses of strata-crossing roadways further reveal nonuniform failure in space and time [8–11]. Coal seam dip, cross-sectional shape, and mining sequence also affect stress redistribution and plastic zone development [12–14]. These findings establish the importance of geological orientation, but the dip of strata and the longitudinal inclination of a roadway represent distinct engineering variables.

Anchorage studies show that bolt–interface intersection angles, host rock strength, and reinforcement properties govern load transfer and resistance to shear deformation [15–17]. Effective anchorage and compatible bolt–cable pretension are consequently important to support performance [18,19]. Targeted reinforcement, roadside filling, grouting, and roof cutting have been applied under different geological conditions [20–23], while sensitivity analysis highlights the role of bolt spacing in controlling weak zones [24]. Under strong mining disturbance, dynamic–static load interaction and disturbance location introduce additional requirements [25,26], prompting coupled anchoring and pressure relief approaches [27,28].

Post-peak rock–support interaction and longitudinal deformation profiles provide further bases for selecting support capacity and installation timing [29,30]. However, these findings do not directly establish a permanent support layout with reduced drilling demand for the present inclined hard rock excavation. A site-specific assessment is needed to connect inclination-dependent stress redistribution, deformation, and plastic zone development with the lengths, spacing, and specifications of reinforcement components. The practical question is whether the support workload can be reduced while maintaining acceptable deformation control under the investigated conditions.

This study examines the lower section of the return air blind inclined shaft at Shunhe Coal Mine. Theoretical analysis and FLAC3D simulations based on measured mechanical parameters evaluate surrounding rock response at six roadway inclination angles between 0° and 25°. The original layout is compared with two optimized support configurations involving adjustments to bolt spacing, cable length, and cable specifications. Numerical results and field displacement monitoring assess deformation control, while total support borehole drilling length per excavation cycle quantifies the construction workload. The study aims to coordinate surrounding rock stability with reduced drilling demand in deep inclined hard rock roadways.

2 Engineering Overview

2.1 Geological Overview

The lower section of the return air blind inclined shaft is an excavation roadway in the west wing of Shunhe Coal Mine. Its designed length is 788.895 m with a semicircular arch cross-section of 5.36 m × 4.08 m. The burial depth ranges from 851.3 m to 1078.3 m, indicating deep mining conditions. The roadway is located in fine sandstone beneath the No. 2_2 coal seam floor. The quartz content is approximately 85%, representing typical hard rock. The strata show a monocline structure, and the apparent dip angle along the excavation direction is 11–25°, with an average value of 17°, which classifies it as a large-inclination roadway. The regional ground pressure ranges from 22.1 MPa to 28.0 MPa, and the geotemperature is 31.6–35.7 °C. Hydrogeological conditions are simple, and risks of gas and coal dust are low. This roadway features deep depth, high ground pressure, hard rock and large inclination, and excavation faces challenges including surrounding rock control, rock breaking and inclined construction. The return air blind inclined shaft is located 11–15 m below the floor of the No. 2_2 coal seam and adopts a circular arch cross-section. The layout of the return air blind inclined shaft is shown in Figure 1, and its stratum column is presented in Figure 2.

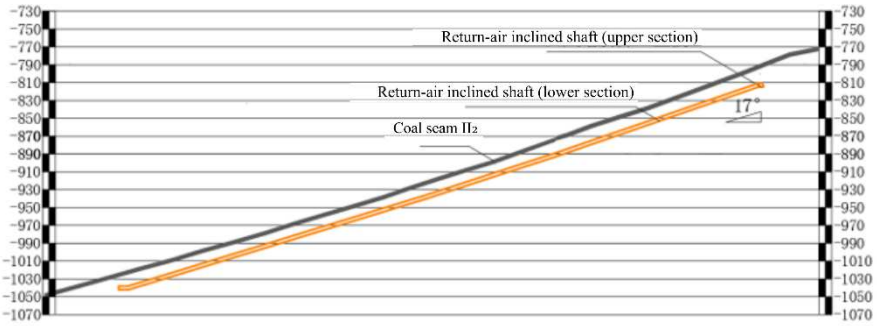


Figure 1 Schematic Cross-section of the Return-air blind Inclined Shaft

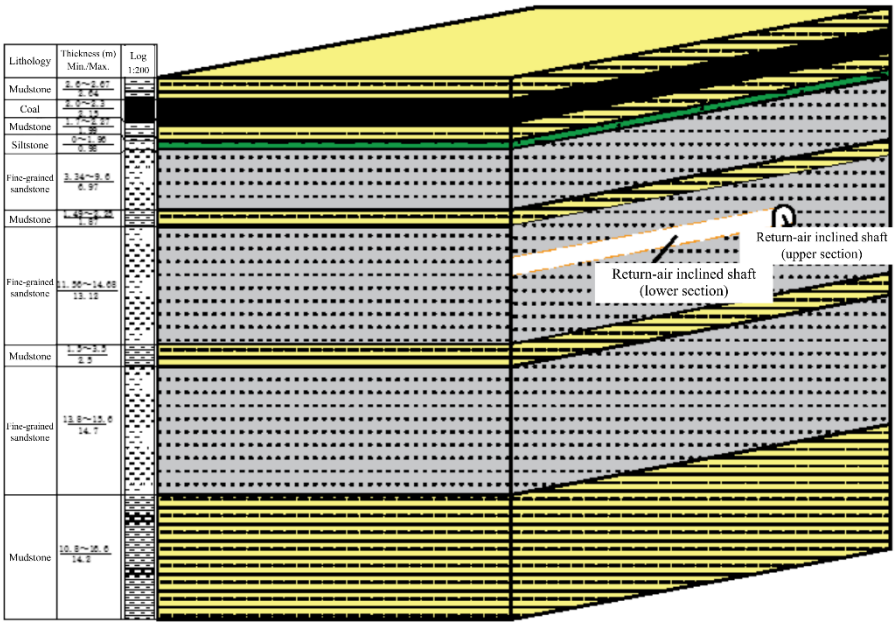


Figure 2 Rock Strata Columnar Section

2.2 Mechanical Analysis of Surrounding Rock in Deep Large-inclination Roadways

2.2.1 Analysis of Surrounding Rock Failure Characteristics of Deep Roadways

High in-situ stress conditions dominate the mechanical response of deep roadways. Excavation essentially triggers dynamic evolution of the surrounding rock stress field from an equilibrium state to drastic reconstruction, leading to strongly nonlinear deformation characteristics. Driven by unloading effects, stress transfers non-uniformly toward the roof and two sidewalls, which readily induces instability hazards such as delamination, roof fall and rib spalling. Especially in fractured rock masses with well-developed joints and faults, the coupling between high stress fields and structural weak planes markedly increases the potential for dynamic disasters. This poses severe challenges to roadway support design and stability control.

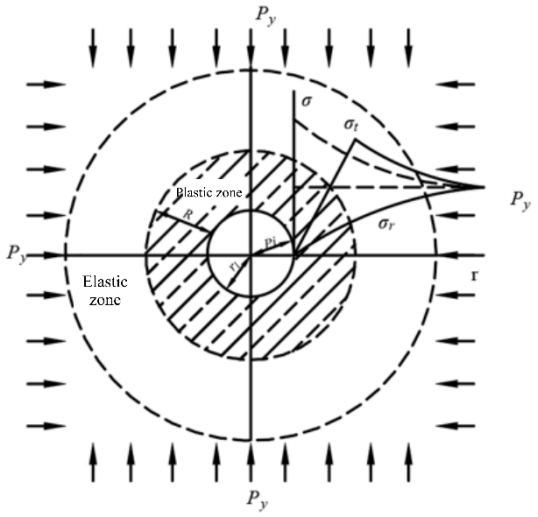


Figure 3 Elastoplastic Deformation Zone of Roadway Surrounding Rock

P_y—in-situ stress; σ_Q—tangential stress; σ_r—radial stress; r_l—radius of the circular roadway; R—radius of the plastic zone; P_i—support resistance.

The roadway is simplified as a circular roadway under uniform confining pressure. Elastic-plastic theory is adopted to calculate the surrounding rock stress, plastic zone radius and peripheral displacement of the roadway.

Displacement in the plastic zone:

$$\mu_r p = \frac{2p(1-\mu^2)}{E}\frac{{R_P}^2}{r_y} - [(Pi + C\cdot cot\varphi)(\frac{R_P}{r_h})^{\frac{2sin\varphi}{1-sin\varphi}} - C\cdot cot\varphi]\frac{1+\mu}{E}\frac{{R_P}^2}{r_y} \quad (1)$$

Radius of the plastic zone:

$$R_P = r_h[\frac{(p+C\cdot cot\varphi)(1-\sin\varphi)}{P_i+C\cdot cot\varphi}]^{\frac{1-sin\varphi}{2sin\varphi}} \quad (2)$$

Stress in the plastic zone:

$${\sigma_r}^p = (Pi + C\cdot cot\varphi)(\frac{\mathrm{r}}{\mathrm{r_h}})^{\frac{1-\sin\varphi}{2\sin\varphi}} + C\cdot cot\varphi \quad (3)$$

$${\sigma_Q}^P = (Pi + C\cdot cot\varphi)(\frac{1+\sin\varphi}{1-\sin\varphi})(\frac{\mathrm{r}}{\mathrm{r_h}})^{\frac{2\sin\varphi}{1-\sin\varphi}} - C\cdot cot\varphi \quad (4)$$

where:

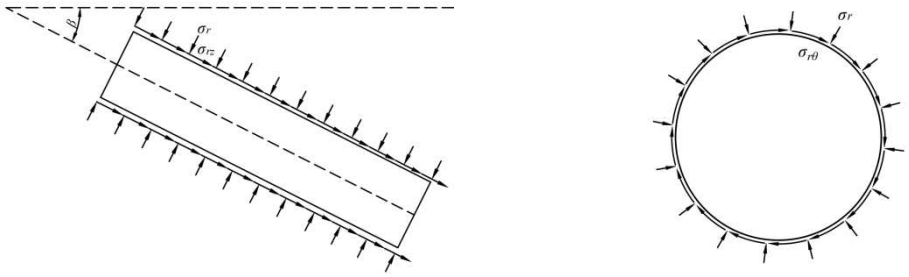
μ—Poisson's ratio; E—elastic modulus, MPa; r_h—roadway radius, m; C—cohesion, Pa; φ—internal friction angle, °.

In-depth analysis of the formulas for plastic zone displacement and radius reveals that the in-situ stress field acts as the decisive variable governing roadway surrounding rock stability and the evolution of peripheral deformation. Tangential stress experiences the most intense disturbance and exhibits obvious coupled growth with the initial stress condition. As mining activities extend deeper underground, the linear rise of in-situ stress causes synchronous intensification of tangential stress. Once the internal stress within surrounding rock exceeds its critical self-bearing limit, instability failures including shotcrete spalling, rock fracturing and large deformation will inevitably occur. These failures severely endanger safety protection and construction schedules.

The surrounding rock deformation law of deep high-stress roadways exhibits remarkable

heterogeneity, which can be summarized in the following three aspects. First, excavation of deep roadways triggers mechanical instability of the original bearing structure. Even with limited variation in radial stress gradient, plastic flow inside rock masses can induce surrounding rock cracking or roof spalling and other failures until a new stress equilibrium state forms through deformation release. Second, such roadways are highly sensitive to the evolution of primary and mining-induced fractures. On one hand, high-stress conditions drive stress concentration and unstable propagation at fracture tips. On the other hand, connected fractures destroy rock mass integrity and allow water and gas erosion to penetrate deeper, accelerating the degradation of mechanical properties of surrounding rock. Finally, excavation disturbance induces the reconstruction of the surrounding rock stress field. As the plastic loosening zone continuously extends deeper, the peripheral displacement of the roadway imposes considerable compressive loads on the support structure. If the bearing capacity and deformation coordination capacity of the support system are insufficient, sequential failure of bolts and cables and large-area roof collapse may readily occur, eventually resulting in roadway support failure and serious threats to construction safety.

2.2.2 Failure Characteristics of Surrounding Rock in Inclined Roadways



(a) Longitudinal section (b) Cross-section

Figure 4 Schematic Diagram of Stress in an Inclined Roadway

Vertical stress of strata:

$$\sigma_v=\gamma_g h \tag{5}$$

Horizontal stress of strata:

$$\sigma_h=\lambda\gamma_g h \tag{6}$$

where:h—depth corresponding to the inclined roadway; γ_g—rock mass unit weight; λ—lateral pressure coefficient of rock and soil;

Expression of surrounding rock stress:

$$\sigma_r=\frac{1}{4}\{1+3K_0+(1-\lambda)[cos2\beta-(1+cos2\beta)cos2\theta]\}\cdot\gamma_g h \tag{7}$$

$$\sigma_{r\theta}=\frac{1}{4}(1-\lambda)(1+cos2\beta)cos2\theta\cdot\gamma_g \mathrm{h} \tag{8}$$

$$\sigma_{rz}=\frac{1}{2}(1-\lambda)sin\theta sin2\beta\cdot\gamma_g(hsin\beta+rcos\beta sin\theta) \tag{9}$$

For horizontal roadways, the angle β between the roadway and the horizontal direction is 0°. Substituting β = 0° into Equations 7 to 9 yields the stress of the horizontal roadway as:

$$\sigma_r=\frac{1}{2}[1+\lambda-(1-\lambda)cos2\theta]\gamma_g h \tag{10}$$

$$\sigma_{r\theta}=\frac{(1-\lambda)sin2\theta\gamma_g h}{2} \tag{11}$$

$$\sigma_{rz}=0 \tag{12}$$

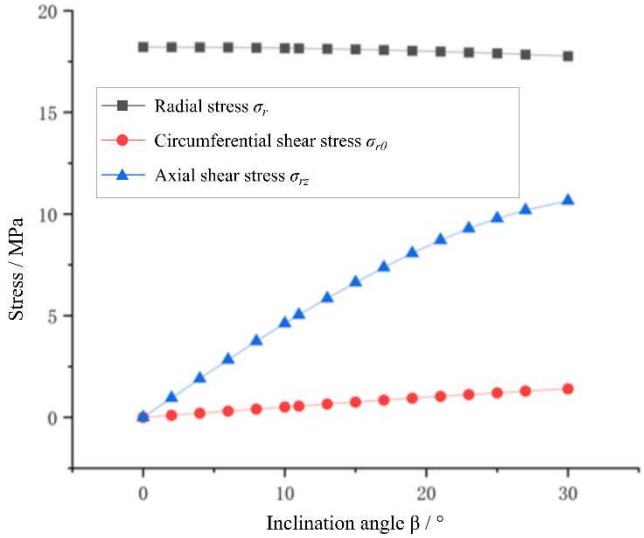


Figure 5 Inclination angle-stress curve

It can be seen from the above formulas that inclined roadways generally have radial stress σr, circumferential shear stress σrθ and axial shear stress σrz, which makes the stress state of inclined roadways more complicated. Compared with horizontal roadways, inclined roadways are governed by additional shear stress along the axial direction and asymmetric loads. The deformation and failure of the roof, floor and two sidewalls show obvious directionality. Conventional uniform support and single bolt support cannot adapt to such complex stress conditions and fail to effectively restrain shear failure and large deformation of surrounding rock. It is necessary to improve the performance of bolts and cables and optimize the rationality of the support system in a targeted manner.

Affected by the roadway dip angle and burial depth, the surrounding rock stress is non-uniformly distributed along both the circumferential and axial directions. The roof and upper side are high stress concentration zones, while the stress on the lower side is relatively low. The surrounding rock is prone to bedding shear slip along the dip direction, roof separation and collapse, as well as bulging and shear failure of the upper side. The deformation and failure exhibit obvious directionality and imbalance. Under the action of combined shear stress, joints and fractures in surrounding rock rapidly propagate and coalesce, which greatly reduces rock mass integrity.The deformation mode transforms from conventional compressive deformation to intensive shear-slip deformation, featuring rapid instability and poor controllability. Conventional support cannot restrain the development of failure.

Therefore, bolts and cables for deep large-inclination roadways need to possess high tensile strength and strong shear resistance, with both radial bearing capacity and axial shear resistance, to

prevent shear fracture of rods and anchorage failure. Bolts and cables with high yield strength and high elongation shall be selected to accommodate the large deformation characteristics of surrounding rock and avoid brittle fracture, ensuring long-term support reliability. High-strength left-handed non-ribbed bolts and steel strand cables are preferred, matched with high-strength pallets, spherical washers and nuts to improve the fitting between pallets and surrounding rock and disperse local stress concentration. W-shaped steel belts or steel beams are adopted as auxiliary components to connect individual bolts and cables into an integrated bearing structure, so as to enhance the integrity and shear resistance of the support system.

3 Analysis of the Influence of Different Dip Angles on Roadways

3.1 Numerical Simulation Scheme

3.1.1 Model Establishment

To simulate the variation of surrounding rock stress and deformation characteristics of steep hard-rock roadways under different dip angles, numerical simulation is carried out to investigate the displacement and stress evolution of hard-rock roadways at six dip angles (0°, 5°, 10°, 15°, 20°, 25°).

The FLAC3D numerical simulation software is used to construct the numerical calculation model based on the stratum occurrence conditions and measured physical and mechanical parameters of rock samples for the lower section of the return air blind inclined shaft in Shunhe Coal Mine. Considering various influencing factors, the model is divided into 10 rock layers. Combined with the stratum column diagram, the model dimension is set as 50 m × 20 m × 67 m . The cross-section of the lower section of the return air blind inclined shaft adopts a semicircular arch shape with width × height = 5.2 × 4.0 m. The boundary conditions of the whole model are as follows: horizontal displacement is constrained on the four lateral boundaries, vertical displacement is fixed at the bottom boundary, and a uniform load equivalent to the gravity of overlying strata (approximately 1040 m thick rock strata) is applied on the top boundary. The calculated load value is 2.5 × 104 × 1040 = 26 MPa. The constraint settings are specified as: the top boundary is a stress boundary, the bottom boundary is fixed in vertical displacement, and the left and right boundaries are fixed in horizontal displacement. The buried depth of the rock roadway in the lower section of the return air blind inclined shaft is about 1000 m, with an applied stress of 25.5 MPa on the upper boundary and a lateral pressure coefficient of 1.

The simulation adopts the original support parameters of the steep hard-rock roadway section in the lower section of the return air blind inclined shaft of Shunhe Coal Mine. The bolt spacing and row spacing are 800 mm × 800 mm. Nine cables are arranged in each row. Among them, one cable at the vault and two cables on each side adopt the specification of Φ21.6 mm × 8300 mm, with a spacing and row spacing of 1300 mm × 2400 mm. One spot cable is installed on each sidewall at 400 mm and 800 mm above the arch springing line. These spot cables are Φ21.6 mm × 5300 mm, with a spacing and row spacing of 1200 mm × 2400 mm. The numerical calculation model is shown in Figure 6.

3.1.2 Selection of Constitutive Model

The three-dimensional numerical model consists of the large-inclination hard-rock roadway and its overlying strata. The Mohr–Coulomb constitutive model is adopted for simulating coal and rock mass, and the double-yield constitutive model is used for the goaf.

Mohr–Coulomb Constitutive Model.

According to theoretical analysis and field experience, the failure of rock mass around the stope during coal seam mining is mainly induced by tensile and shear stresses. Therefore, the Mohr–Coulomb yield criterion is adopted in the model calculation:

$$f_s=\sigma_1-\sigma_3\frac{1+sin\varphi}{1-sin\varphi}+2c\sqrt{\frac{1+sin\varphi}{1-sin\varphi}} \tag{13}$$

where: σ1 and σ3 are the maximum principal stress and minimum principal stress, respectively; c and φ denote the cohesion and internal friction angle of the material. The criterion for shear failure is defined as the judgment coefficient fs < 0. Considering the brittle evolution characteristics of coal and rock mass under low stress fields, a tensile strength threshold is additionally set to identify tensile failure. The model calculation is divided into two logical stages: the initial stress field under in-situ stratum conditions is solved in advance, and then numerical simulation of the excavation process of the large-inclination hard-rock roadway is carried out on this basis.

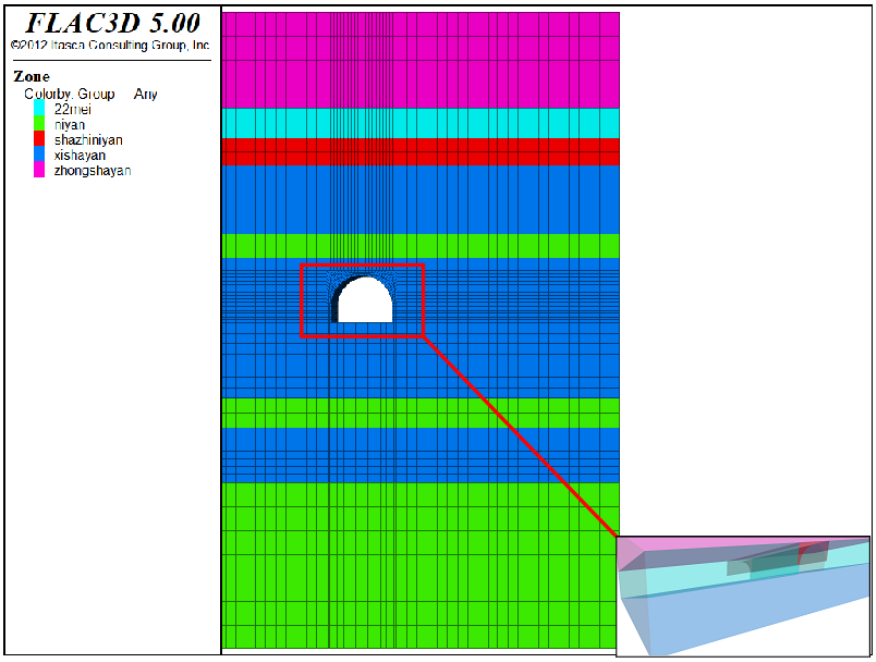


Figure 6 Numerical Calculation Model Diagram

Table 1 Mechanical Parameters of Roadway Surrounding Rock Mass

Lithology	Thickness / m	*Rc* / MPa	*Rt* / MPa	*S* / GPa	*B* / GPa	μ	*C* / MPa	φ /°	γ / kg / m^3
Medium sandstone	8.2	68	5.2	10.3	12.3	0.27	6.6	36	2770

Coal Seam 22	2.3	21	2	0.38	1.19	0.13	1.4	28	1400
Mudstone	2	34	1.8	1.56	3.03	0.14	9.6	36	2660
Sandy mudstone	2.3	28	2.7	1.56	3.03	0.25	9.6	33	2600
Fine sandstone	5.9	65.4	5.6	4.58	5.1	0.28	14.5	40	2650
Mudstone	2	34	1.8	1.56	3.03	0.14	9.6	36	2660
Fine sandstone (roadway)	23	78.8	5.2	4.06	5.1	0.22	9.39	44.12	2650
Mudstone	2.5	34	1.8	1.56	3.03	0.14	9.6	36	2660
Fine sandstone	4.7	65.4	5.6	4.58	5.1	0.28	14.5	40	2650
Mudstone	14.2	34	1.8	1.56	3.03	0.14	9.6	36	2660

3.2 Simulation Analysis of Roadway Deformation Variation under Different Dip Angles

(1) Analysis of the variation of roof-to-floor convergence with roadway dip angle

As the roadway dip angle increases, the roof-to-floor convergence presents a trend of first increasing and then decreasing. When the dip angle ranges from 0° to 5°, the roof-to-floor convergence rises with the increase of dip angle. When the dip angle ranges from 5° to 25°, the roof-to-floor convergence decreases as the dip angle increases. The roof-to-floor convergence at different dip angles is shown in Figure 7, and the variation curve of roof-to-floor convergence versus dip angle is shown in Figure 8.

The roof subsidence exhibits a unimodal characteristic of first increasing and then decreasing with the rise of dip angle, dropping from 21.5 mm at 0° to 18.6 mm at 25°. Increasing the dip angle can effectively restrain the vertical subsidence of roof strata. The floor heave shows an asymmetric characteristic of sharp initial growth followed by continuous reduction, reaching a peak value of 42.7 mm at 5°, which is 2.3 times that under the 0° condition, and then gradually decreases with the increase of dip angle. The total roof-to-floor convergence presents a unimodal distribution of "rising first and then falling", peaking at 63.5 mm at 5°. When the dip angle exceeds 5°, the total convergence continuously decreases and falls to 35.1 mm at 25°, corresponding to the optimal overall stability of surrounding rock.

Under small dip angles, the vertical compressive stress of surrounding rock is strongly coupled with interlayer shear stress. Plastic dilation and shear failure easily occur in floor strata, thereby triggering severe floor heave which dominates the growth of total deformation. As the roadway dip angle increases, the component of rock mass gravity along the bedding plane gradually rises while vertical compression weakens. The stress redistribution of surrounding rock tends to be uniform, roof subsidence and floor heave are simultaneously controlled, and the vertical deformation of surrounding rock gradually converges with the increase of dip angle.

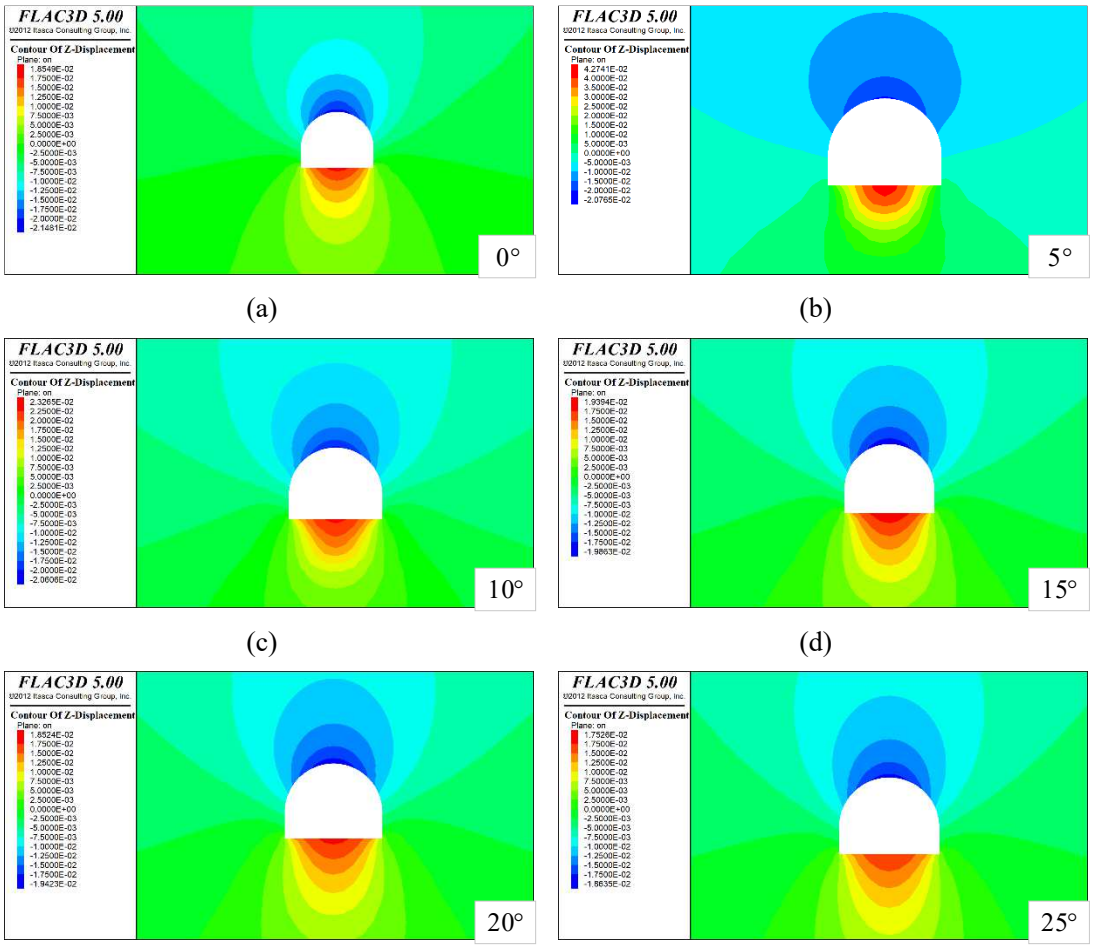


Figure 7 Variation Law of Roadway Roof-to-Floor Convergence with Inclination Angle

Table 2 Vertical Roof-to-Floor Convergence of Surrounding Rock for Roadways with Different Inclination Angles

Roadway dip angle / °	0	5	10	15	20	25
Roof subsidence / mm	21.5	20.8	20.6	19.9	19.4	18.6
Floor heave / mm	18.5	42.7	23.3	19.4	18.5	17.5
Roof-to-floor convergence / mm	40	63.5	43.9	39.3	37.9	35.1

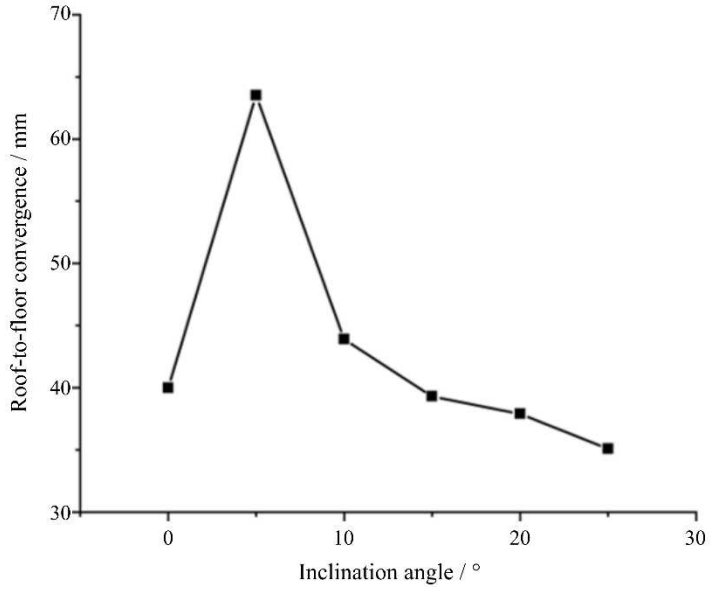


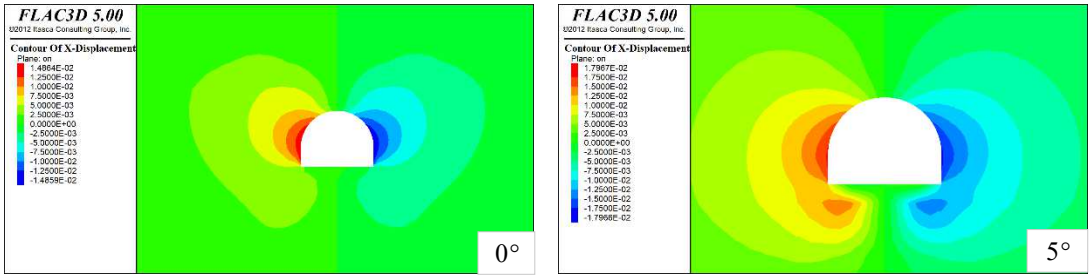
Figure 8 Variation Curve of Roadway Roof-to-Floor Convergence with Increasing Inclination Angle

(2) Analysis of the variation of sidewall convergence with roadway dip angle

The sidewall convergence of the roadway at different dip angles is shown in Figure 9. The sidewall convergence of roadway surrounding rock under various dip angles is listed in Table 3, and the variation curve of sidewall convergence with increasing dip angle is presented in Figure 10.

It can be seen from Figure 9 that the overall roadway deformation is approximately symmetrically distributed. As the roadway dip angle increases, the sidewall convergence shows a trend of first increasing and then decreasing. When the dip angle ranges from 0° to 5°, the sidewall convergence rises with the increase of dip angle. When the dip angle ranges from 5° to 25°, the sidewall convergence decreases as the dip angle increases. The total sidewall convergence reaches its peak value of 35.9 mm at 5°. With the further increase of dip angle, the total convergence continuously decreases and reaches the minimum value of 27.0 mm at 25°, indicating that the lateral convergence deformation of roadway surrounding rock is effectively controlled.

Under small dip angles, the horizontal stress of surrounding rock is unevenly distributed. Shear slip and plastic extrusion easily occur in the sidewall rock mass, resulting in a rapid rise in convergence. When the dip angle exceeds 5°, the gravitational stress of strata is decomposed along the dip direction, the horizontal lateral compression weakens, the stress state of surrounding rock tends to be uniform, and the sidewall convergence deformation gradually decreases with the increase of dip angle.



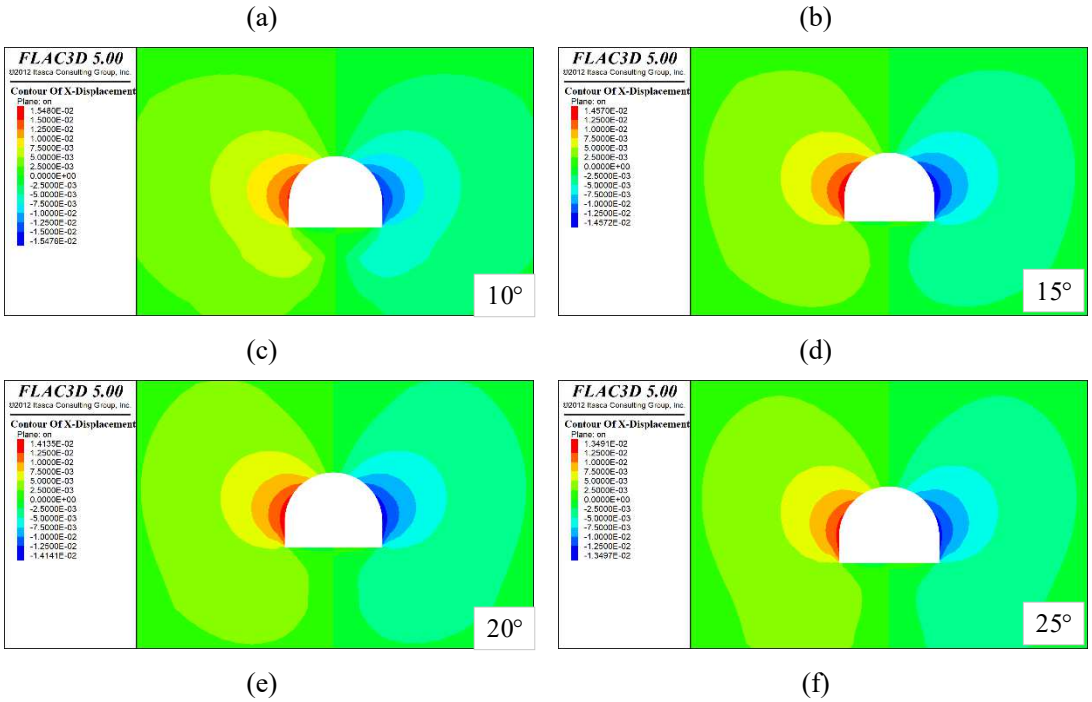


Figure 9 Variation law of convergence of two sides of roadway with increasing inclination angle

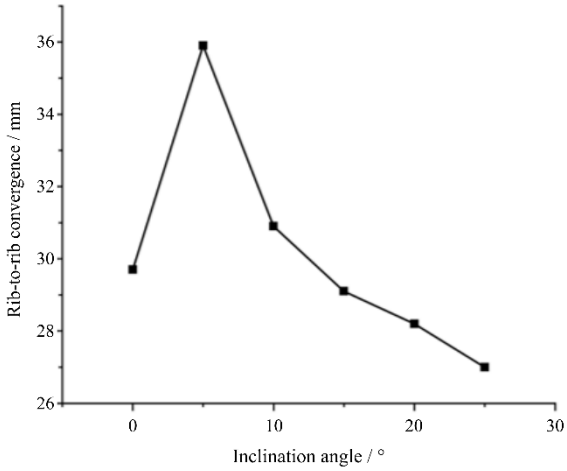


Figure 10 Variation curve of convergence of the two sidewalls with increasing inclination angle

Table 3 Two-Side Convergence of Roadway Surrounding Rock Under Different Inclination Angles

Roadway dip angle / °	0	5	10	15	20	25
Left sidewall convergence / mm	14.9	18	15.5	14.6	14.1	13.5
Right sidewall convergence / mm	14.8	17.9	15.4	14.5	14.1	13.5
Sidewall convergence / mm	29.7	35.9	30.9	29.1	28.2	27

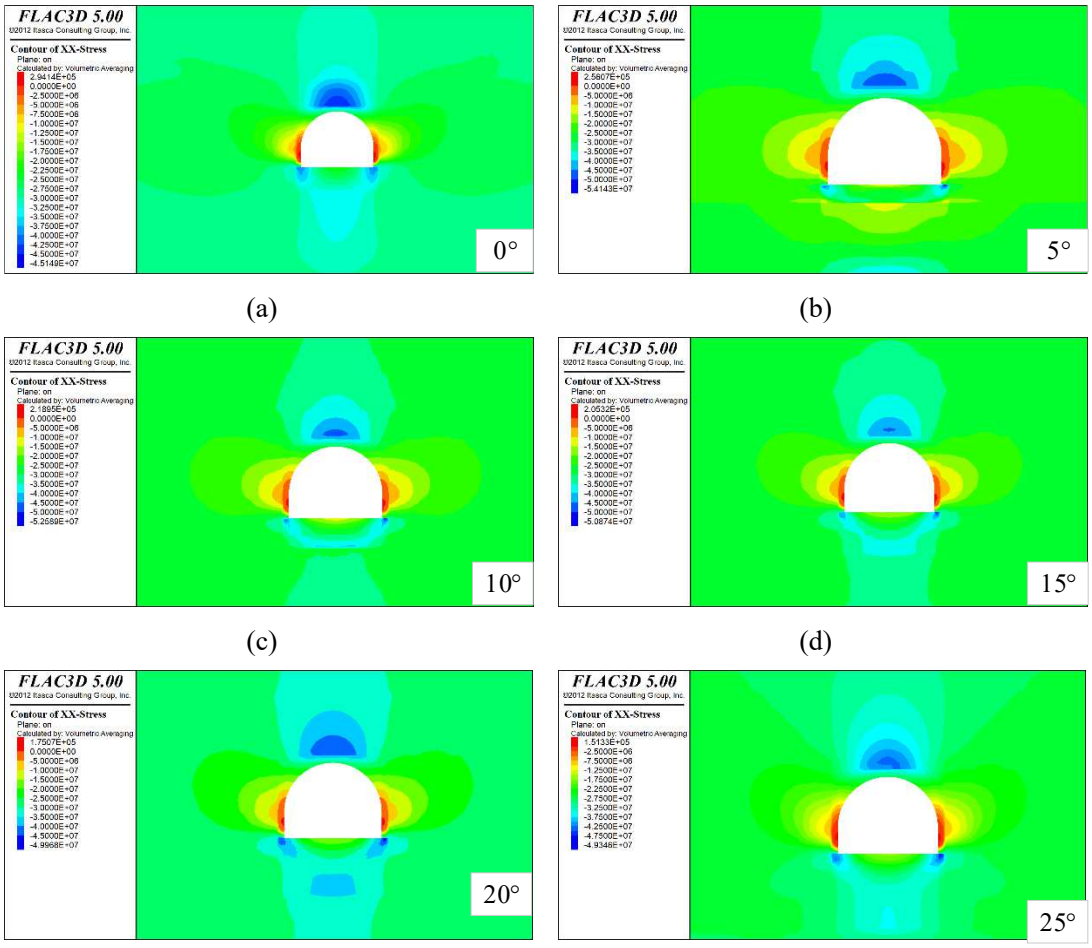
(3)Analysis of variation of roadway horizontal stress with dip angle

The horizontal stress data obtained along the upward 10 m line starting from the center of the roadway roof is shown in Figure 11. The contour nephogram of horizontal stress in surrounding rock above the roadway and its variation curve with increasing dip angle are presented in Figure 12.

It can be observed from Figure 11 and Figure 12 that the horizontal stress nephograms under different dip angles show that the surrounding rock around the roadway exhibits the highest degree

of stress concentration under the 0° condition, with a widely distributed high-stress zone and large stress gradient. As the dip angle gradually increases, the overall horizontal stress of surrounding rock continuously decreases, the stress concentration is remarkably alleviated, the high-stress region shrinks constantly, and the stress distribution becomes uniform and gentle. The variation curve of horizontal stress in surrounding rock above the roadway further demonstrates that the roof stress value decreases monotonically with the increase of dip angle. A larger dip angle corresponds to weaker roof stress concentration and a more stable stress environment. When the dip angle rises to 25°, the overall horizontal stress of the roadway reaches the minimum, the uniformity of stress distribution is optimal, and the stress state of surrounding rock is significantly improved.

Under small dip angles, the gravity of strata mainly acts as vertical compression, leading to intensive accumulation of horizontal stress and easy formation of stress concentration zones around the roadway. As the roadway dip angle increases, the decomposition of rock mass gravitational stress along bedding and dip directions is enhanced, vertical compression and horizontal lateral restraint are weakened, and the stress redistribution of surrounding rock becomes more coordinated, which effectively reduces the peak value and concentration degree of horizontal stress. The above results indicate that the increase of roadway dip angle can optimize the stress state of surrounding rock and restrain stress concentration, providing an important theoretical basis for stability control and support scheme design of inclined roadway surrounding rock.



(e) (f)

Figure 11 Horizontal Stress Nephogram of Roadway Surrounding Rock with Increasing Inclination Angle

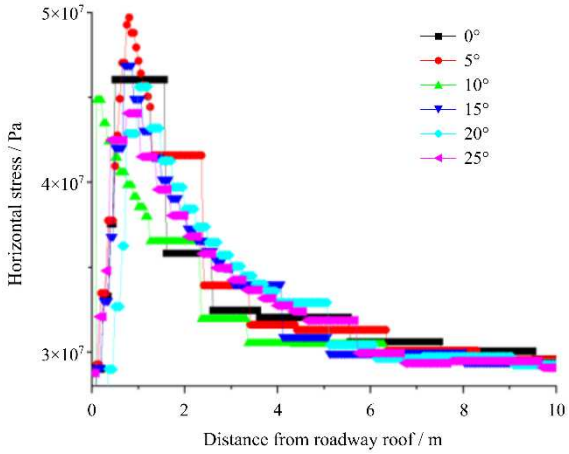


Figure 12 Variation Curve of Horizontal Stress Nephogram of Roadway Top Surrounding Rock with Increasing Inclination Angle

(4) Analysis of variation of roadway vertical stress with dip angle

The vertical stress data within 10 m upward from the center of the roadway roof are shown in Figure 13. It can be seen from Figure 13 that the dip angle is a key parameter affecting the magnitude and distribution pattern of vertical stress in surrounding rock, and the degree of stress concentration shows a significant weakening trend with the increase of dip angle.

According to the vertical stress nephograms of surrounding rock under different dip angles, the vertical stress concentration of roadway surrounding rock is the most prominent under the 0° working condition, with a widely distributed high-stress zone and large stress gradient, and the surrounding rock is subjected to intense vertical compression. As the roadway dip angle gradually increases, the decomposition effect of stratum gravitational stress along the dip direction keeps strengthening, the vertical compression component continuously decreases, and the peak vertical stress and the scope of high-stress zone of surrounding rock reduce simultaneously. When the dip angle increases from 5° to 25°, the vertical stress distribution gradually becomes uniform and gentle, and the stress concentration is continuously alleviated. Under the 25° working condition, the vertical stress of surrounding rock is the minimum and the overall stress state is the most stable.

Under small dip angles, rock mass gravity is dominated by vertical loading. High stress concentration zones are easily formed at the roof, floor and sidewalls of the roadway, which increases the risk of plastic failure of surrounding rock. As the dip angle increases, the vertical component of gravitational stress decreases while the tangential component rises, making the stress redistribution of surrounding rock more coordinated and effectively reducing the degree of vertical stress concentration. The above laws demonstrate that increasing roadway dip angle can significantly optimize the vertical stress environment of surrounding rock, which provides important theoretical basis and data support for surrounding rock control and support parameter design of inclined roadways.

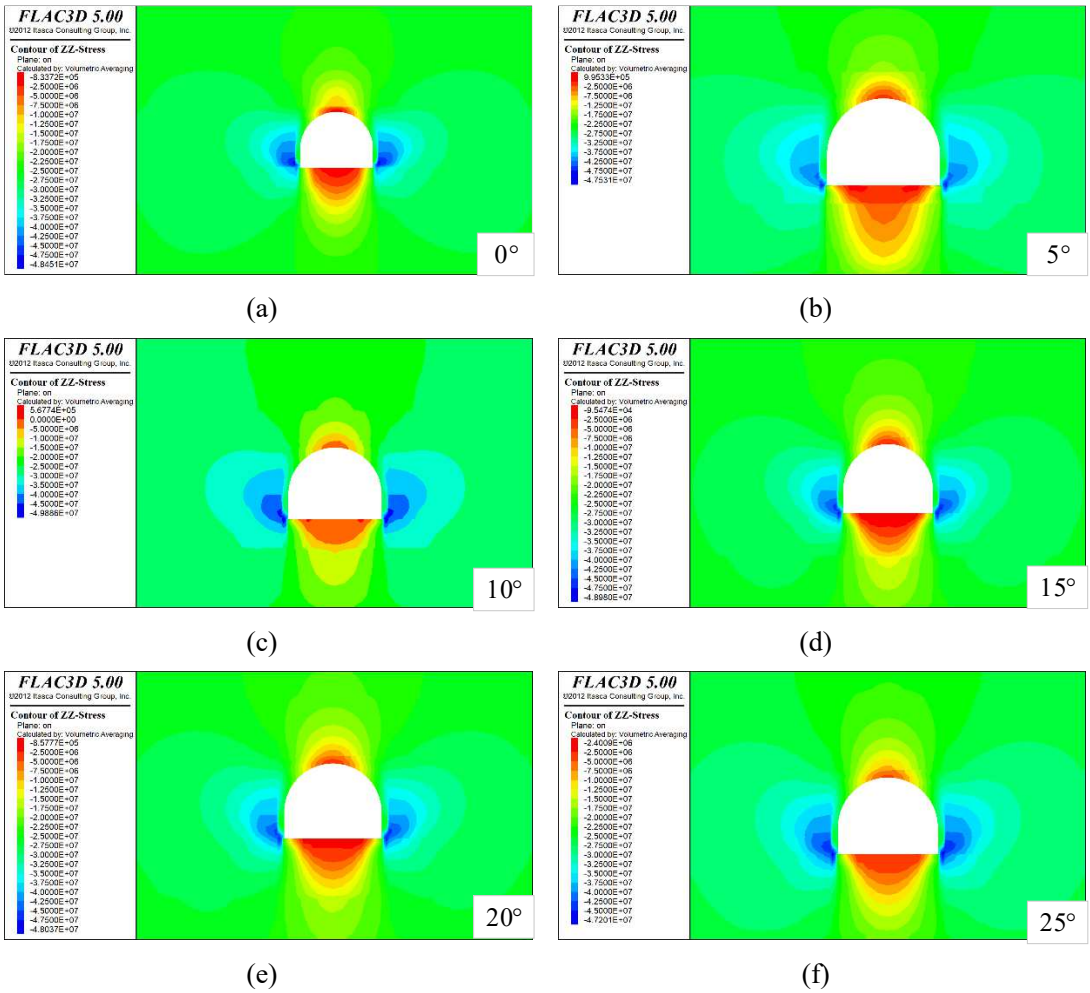


Figure 13 Variation Curve of Vertical Stress Nephogram of Roadway Surrounding Rock with Increasing Inclination Angle

(5) Analysis of plastic zone variation of roadway surrounding rock under different dip angles

The shear stress generated by the stratum tilting effect can change the distribution pattern of the surrounding rock plastic zone. It can be seen from Figure 14 that the additional shear stress induced by stratum inclination is a key mechanical factor governing the shape and range of the surrounding rock plastic zone. The roadway plastic zone presents a unimodal evolution law of first expanding and then contracting with the increase of dip angle.

When the dip angle increases from 0° to 5°, the additional shear stress of surrounding rock continuously rises, the shear failure degree of rock mass intensifies, and the plastic zone gradually expands with the increase of dip angle. When the dip angle exceeds 5°, with the further increase of roadway dip angle, the stress redistribution of surrounding rock tends to be coordinated, the shear failure effect gradually weakens, and the development range of the plastic zone keeps shrinking. It can be seen from the plastic zone distribution nephograms that the through range of surrounding rock plastic zone reaches the maximum under the 5° working condition, which is the critical dip angle for the plastic zone to transit from expansion to contraction. When the dip angle increases to 25°, the surrounding rock plastic zone is the smallest with the most concentrated distribution, and the integrity and stability of rock mass are significantly improved.

Under small dip angles, the gravity of strata is dominated by vertical compression, leading to remarkable stress concentration in surrounding rock and easy occurrence of extensive shear plastic failure. As the dip angle increases, gravitational stress is decomposed along the bedding and dip directions, vertical compression and shear effects are weakened, and the development of the surrounding rock plastic zone is effectively restrained.

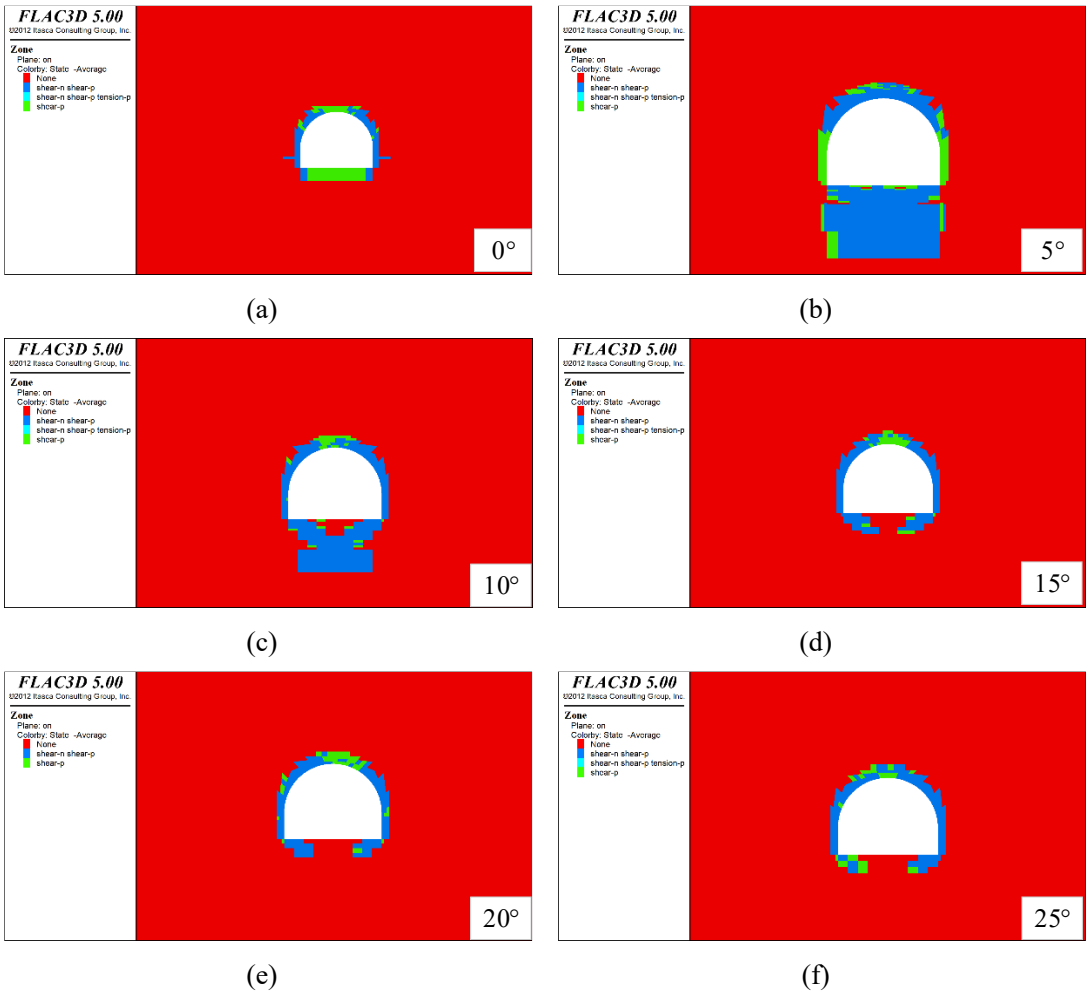


Figure 14 Variation Law of Roadway Plastic Zone with Increasing Inclination Angle

Roadway dip angle is a key factor controlling the mechanical response of surrounding rock in deep hard-rock roadways. The surrounding rock deformation, stress distribution and plastic zone range all exhibit a unimodal evolution characteristic of first increasing and then decreasing with the rise of dip angle, and 5° serves as the critical inflection point for deformation and failure. In the range of 0° to 5°, under the coupling effect of additional shear stress and vertical compression, the roof-floor and sidewall convergences increase rapidly, stress concentration is prominent, and the plastic zone expands continuously. In the range of 5° to 25°, as gravitational stress decomposes along the dip direction, vertical and horizontal stress concentrations gradually weaken, the deformation continuously decreases, and the plastic zone keeps contracting. Under the 25° working condition, the roadway surrounding rock has the minimum deformation, the most uniform stress distribution and the smallest plastic zone range, achieving the optimal stability.

Therefore, the bolts and cables required for support should possess both high tensile strength

and strong shear resistance, with consideration of radial bearing capacity and axial shear resistance, to prevent shear fracture of the rod and anchorage failure. Bolts and cables with high yield strength and high elongation shall be selected to accommodate the large deformation characteristics of surrounding rock, avoid brittle fracture, and guarantee long-term support reliability.

4 Optimization Design of Support Scheme for Deep Large-inclination Roadway

4.1 Original Support Scheme

The support form of "bolt-mesh-shotcrete + cable" is adopted for the roadway section of the lower section of the return air blind inclined shaft. A total of 15 high-strength left-handed threaded steel bolts (HRB500) with specification Φ22 mm × 2400 mm are arranged on the full section at a spacing and row spacing of 800 mm × 800 mm. Nine cables are installed in each row: one cable at the vault plus two cables on each side are 1 × 7 strand cables with specification Φ21.6 mm × 8300 mm at a spacing and row spacing of 1300 mm × 1600 mm. An arched beam is mounted at the center of the roof. One spot cable is constructed on each sidewall at 400 mm and 800 mm above the arch springing line, with specification Φ21.6 mm × 5300 mm and spacing and row spacing of 1200 mm × 1600 mm. The support section drawing is shown in Figure 15.

4.2 Optimized Support Scheme

Based on the above analysis of roadway responses under different dip angles, aiming at the characteristics of the hard-rock roadway with a dip angle of 17°, where a stable asymmetric bearing arch has been formed in surrounding rock and the plastic zone is relatively uniform and shallow, a precision support strategy of strengthening key positions and simplifying non-critical areas should be adopted. On the premise of guaranteeing safety and stability, support density can be reduced by optimizing support parameters to improve excavation efficiency.

In the original scheme, the central roof area lies within the protection zone of the bearing arch under the 17° dip angle with low vertical stress. The bolts in this region bear little force and make limited contributions, serving merely as "safety redundancy". Removing these bolts will not impair the overall stability of the roof; on the contrary, it can accelerate the support construction speed and reduce material consumption.

Cables function to suspend shallow unstable rock strata onto deep stable rock masses. The plastic zone analysis in Chapter 2 indicates that under the 17° dip angle, the plastic zone of surrounding rock only develops around the roadway. In the optimized scheme, the length of partial cables is shortened from 8.3 m and 5.3 m to 4.3 m, ensuring that their anchorage sections are fully embedded in undisturbed stable rock mass. This measure significantly cuts cable material consumption while maintaining effective suspension effect, reflecting the rationality of design based on accurate surrounding rock response.

Therefore, the bolt spacing and row spacing are adjusted to 1000 mm × 1000 mm with a bolt specification of Φ22 mm × 4300 mm. The original 1 × 7 strand cables of Φ21.8 mm are replaced

by 1 × 19 strand steel strand cables of Φ21.8 mm. Among them, one cable at the vault and one cable on each side adopt the specification of 1 × 19 strand Φ21.8 mm × 8300 mm, with spacing and row spacing of 2600 mm × 2000 mm. Between these three Φ21.8 mm × 8300 mm cables are two Φ21.8 mm × 4300 mm cables. A total of two 4.3 m-long cables are arranged on the roadway sidewalls. One spot cable of 1 × 19 strand Φ21.8 mm × 4300 mm is installed on each sidewall at 800 mm below the arch springing line, with spacing and row spacing of 1200 mm and 2600 mm × 2000 mm. A new high-strength special plum-type anchor-cable pallet with dimensions of length × width × thickness = 300 mm × 300 mm × 8 mm is adopted. This pallet can reduce its thickness while ensuring structural strength and cut the support cost. The optimized support section drawings are shown in Figure 16 and Figure 17.

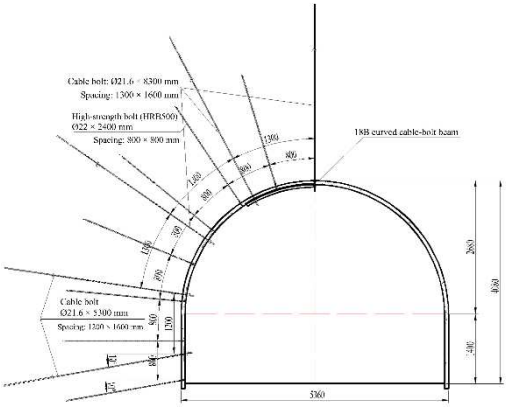


Figure 15 Cross-section of the Original Support Scheme

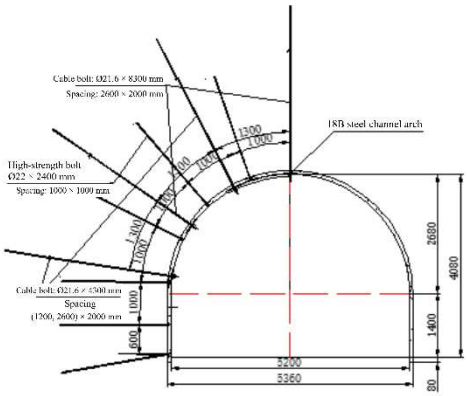


Figure 16 Cross-section of the Optimized Support Scheme 1

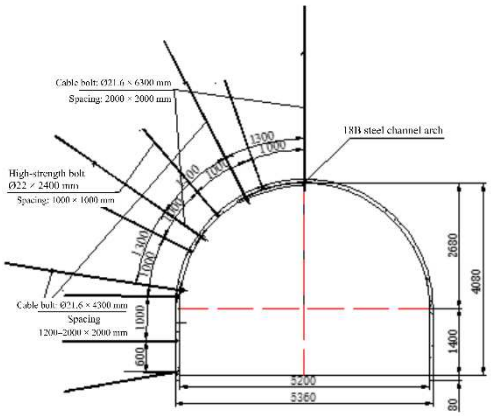


Figure 17 Cross-section diagram of support for Optimization Scheme 2

4.3 Support Simulation Analysis

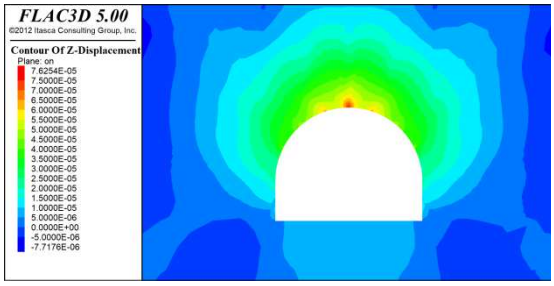
To compare and analyze the control effects of different support schemes, FLAC3D 5.0 software was adopted to establish a three-dimensional numerical model reflecting the geological conditions of deep large-inclination roadways. The model was built based on field geomechanical parameters. After applying the initial in-situ stress field and completing roadway excavation, the construction processes of the original support scheme and the optimized support scheme were simulated respectively. The vertical displacement nephograms, vertical stress distribution diagrams and plastic

zone nephograms under the two schemes were obtained. It can be seen that compared with the original scheme, the optimized scheme can significantly improve the stress state of surrounding rock. Specifically, the convergence value of vertical displacement of roadway roof and floor is greatly reduced; vertical stress concentration transfers from shallow rock to deep rock with a decreased peak value; the range of surrounding rock plastic zone shrinks obviously. In particular, the shear plastic zone at sidewalls and corners is effectively controlled with more uniform and discontinuous distribution, which indicates that the optimized support system can control surrounding rock deformation, improve stress environment and enhance overall stability more effectively. The comparison of specific values and nephograms is shown in Figure 18.

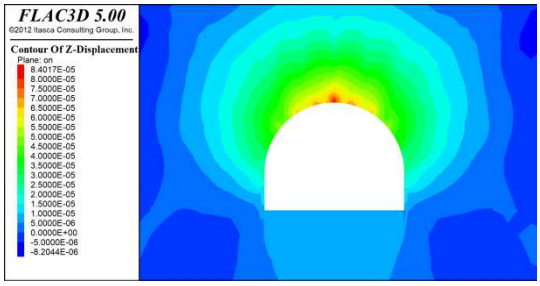
Figure 18 shows the comparison of vertical displacement nephograms of roadway surrounding rock under the original support scheme and two optimized schemes. It can be seen from the figure that the vertical displacement of surrounding rock under each scheme presents the distribution law of vault subsidence and floor heave. The influence range of displacement is concentrated around the roadway and gradually attenuates towards deep surrounding rock, which conforms to the basic mechanical characteristics of surrounding rock deformation after excavation of soft rock roadway.

The peak vertical displacement of the original scheme is obviously higher, the high-displacement zones of roof and floor are widely distributed, and the trend of vertical convergence is prominent. By enlarging bolt spacing and row spacing and adjusting the specification and layout of anchor cables, Optimization Scheme 1 greatly reduces the displacement peak, the scope of high-displacement zone shrinks remarkably, and the vertical deformation of roof and floor is effectively restrained. After removing the two anchor cables at the floor corners on the basis of Scheme 1, Optimization Scheme 2 sees a slight rise in displacement amplitude, but the overall value is still much lower than that of the original scheme. The high-displacement zone does not expand obviously, and the vertical deformation remains within the controllable range.

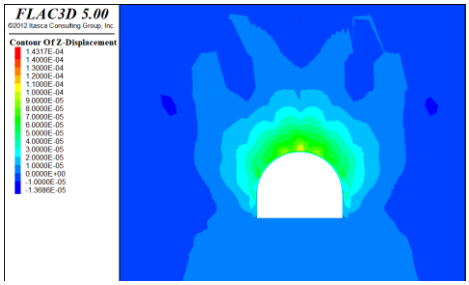
The vertical displacement of surrounding rock in each scheme shows a trend of “rising rapidly to the peak within 2 m from the roadway surface, and then gradually attenuating to nearly zero with the increase of depth”, which is consistent with the typical characteristic that deformation of deep roadways diffuses and attenuates towards deep rock mass. For the original scheme, deformation concentrates in shallow rock with a large gradient, which easily induces local subsidence failure at the vault. By slowing the deformation attenuation rate and expanding the influence range, the optimized schemes achieve more uniform deformation distribution and a markedly reduced gradient, effectively restraining the local concentrated subsidence effect and greatly improving the surrounding rock stability of deep large-inclination roadways.



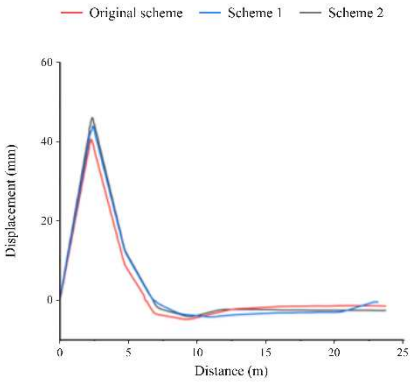
(a) Vertical Displacement Nephogram of Roadway under the Original Scheme



(b) Vertical Displacement Nephogram of Roadway under Optimization Scheme 1



(c) Vertical Displacement Nephogram of Roadway under Optimization Scheme 2



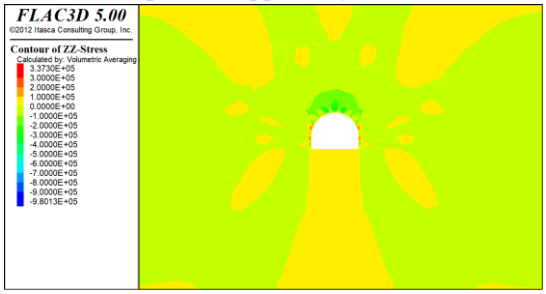
(d) Vertical Displacement Curve of Roadway

Figure 18 Vertical Displacement Nephogram

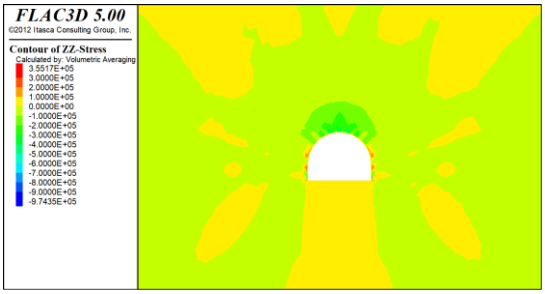
Figure 19 presents the comparison of vertical stress nephograms of roadway surrounding rock under the original scheme and optimized schemes. It can be observed that the vertical stress of roadway surrounding rock under both schemes follows the distribution law of compressive stress concentration at the vault and sidewalls as well as stress release at the floor. The stress concentration zones are mainly distributed along the roadway contour and gradually transition to the in-situ stress level in deep surrounding rock, which conforms to the basic characteristics of stress redistribution after excavation of deep soft rock roadways.

It can be seen from the vertical stress nephograms that the surrounding rock under the original scheme has poor uniformity of vertical stress distribution and remarkable stress concentration, with the maximum vertical stress reaching 3.3730×10^5 Pa. The high-stress zone distributes closely along the roadway contour, which easily induces local shear failure of surrounding rock. By adjusting support parameters, Optimization Scheme 1 realizes reasonable stress reconstruction, and its maximum vertical stress is 3.5517×10^5 Pa. Although slightly increased, the stress distribution becomes more uniform, and the high-stress zone transfers to deep surrounding rock to form a stable bearing structure. After removing the anchor cables at floor corners in Optimization Scheme 2, the maximum vertical stress drops to 3.2525×10^5 Pa, the degree of stress concentration is further weakened, the range of high-stress zone shrinks with gentle gradient, and no abrupt stress change

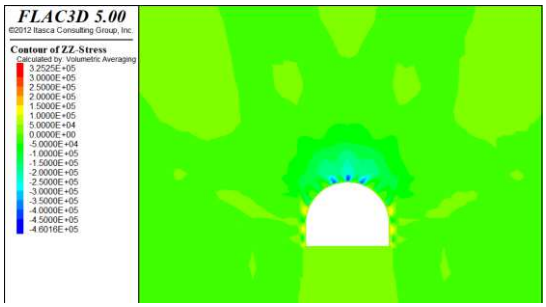
occurs due to partial support adjustment.



(a) Vertical Stress Nephogram of Roadway under the Original Scheme



(b) Vertical Stress Nephogram of Roadway under the Optimized Scheme



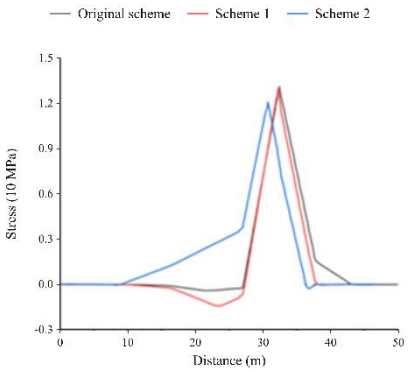
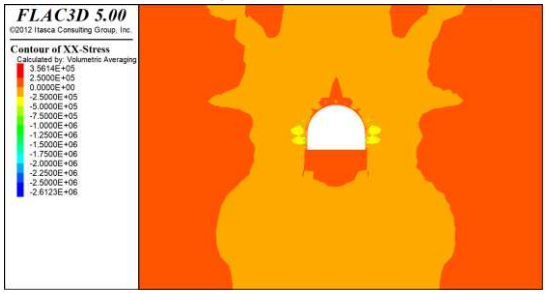


Figure 19 Vertical Stress Distribution Diagram

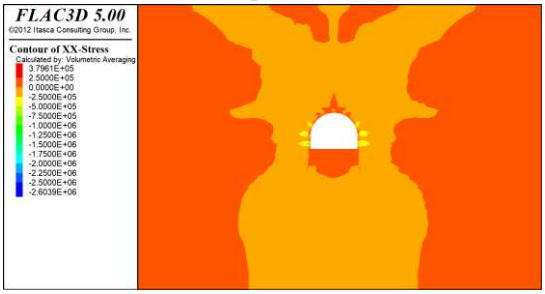
Figure 20 shows the comparison of horizontal stress nephograms of roadway surrounding rock under the original scheme and optimized schemes. Under the original support scheme, the horizontal stress of surrounding rock is unevenly distributed with obvious stress concentration. The high-stress zone is distributed along the roadway contour with a steep stress gradient, which easily induces shear slip failure of rock mass in two sidewalls. By adjusting support parameters, Optimization Scheme 1 achieves the reconstruction of horizontal stress. The maximum horizontal stress increases slightly, while the distribution becomes more uniform, and the high-stress zone transfers to deep surrounding rock to form a stable lateral bearing structure. After adjusting the support layout on the basis of Optimization Scheme 1, Optimization Scheme 2 has a maximum horizontal stress of 3.7815 $\times 10^5$ Pa, which is close to that of Scheme 1. The scope of the high-stress zone shrinks significantly with a gentle stress distribution gradient, and no abrupt stress change or local stress concentration occurs due to the adjustment of support form.

The horizontal stress distribution curve intuitively presents the evolution characteristics of stress with distance: the stress of the original scheme attenuates sharply with the increase of depth, and the stress concentration in shallow surrounding rock is prominent. The stress curves of the two optimized schemes are gentler, gradually decaying to a stable value within the depth range of 0~20 m, which effectively avoids the risk of surrounding rock failure caused by local sharp stress rise. By regulating the transfer path of horizontal stress, the optimized support schemes weaken the stress

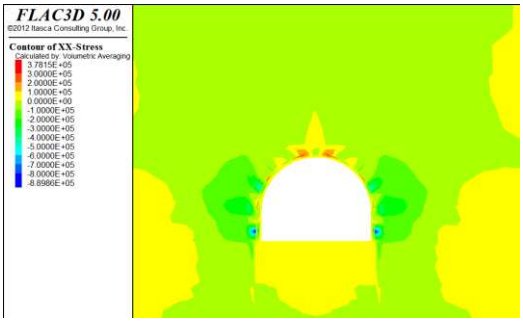
concentration effect around the roadway and optimize the stress state of surrounding rock, providing reliable mechanical guarantee for the stability control of sidewalls in deep roadways.



(a) Horizontal Stress Nephogram of Roadway under the Original Scheme



(b) Horizontal Stress Nephogram of Roadway under the Optimized Scheme



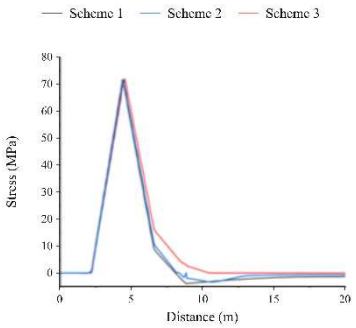
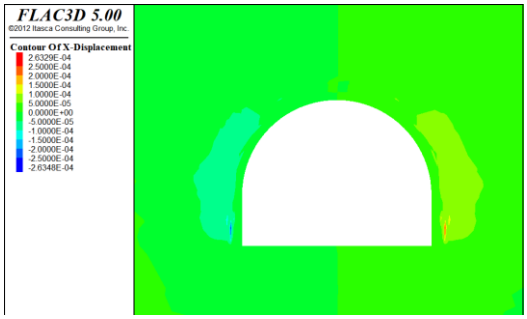


Figure 20 Horizontal Stress Distribution Contour

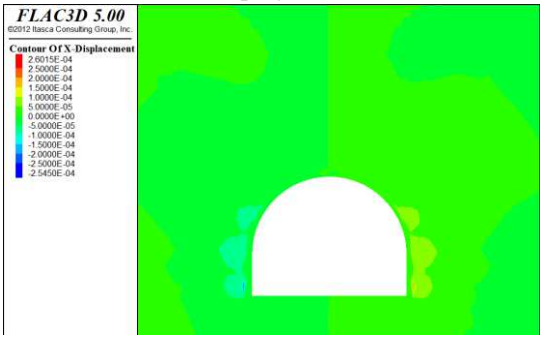
Figure 21 shows the comparison of horizontal displacement nephograms of roadway surrounding rock under the original scheme and optimized schemes. The horizontal displacement nephograms intuitively indicate that the peak horizontal displacement of surrounding rock under the original scheme is remarkably high, reaching 0.263 mm. The high-displacement zone is widely distributed along the two sidewalls of the roadway with a steep displacement gradient, and the lateral extrusion deformation of sidewalls is prominent, which is adverse to the lateral stability of the roadway. By adjusting support parameters and layout, Optimization Scheme 1 effectively restrains lateral deformation. The peak horizontal displacement decreases to 0.108 mm, the range of high-displacement zone shrinks significantly, and the displacement distribution is uniform with a gentle gradient, showing favorable deformation restraint performance. The horizontal displacement nephogram of Optimization Scheme 2 presents slightly larger values at the floor corners, while the high-displacement zones of the two sidewalls do not expand. The lateral deformation is uniform and controllable, verifying that this scheme can maintain excellent lateral deformation control performance while simplifying construction.

The horizontal displacement distribution curves further quantify the deformation evolution law of each scheme. The abscissa covers the depth range of 0~10 m. The curve of the original scheme remains at a high level throughout, the displacement attenuates sharply with increasing depth, and the concentration of shallow lateral deformation is prominent. The curves of the two optimized

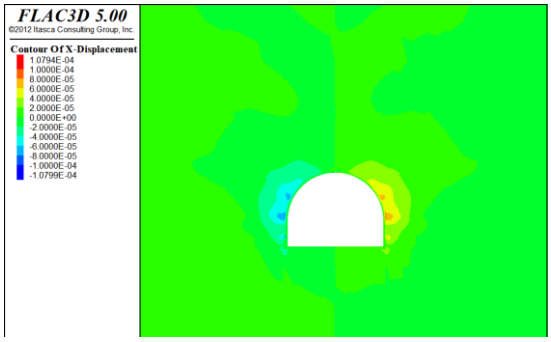
schemes stay at low levels with gentle deformation trends, and no obvious abrupt change occurs in the whole depth range, which effectively avoids the risk of sidewall instability induced by local deformation concentration. In summary, by reconstructing the lateral bearing structure of surrounding rock, the optimized support schemes significantly reduce the peak horizontal displacement and deformation gradient, effectively restrain the lateral convergence deformation of sidewalls, provide reliable guarantee for improving the lateral stability of deep roadways, and offer data support for quantitative optimization of support schemes in similar projects.



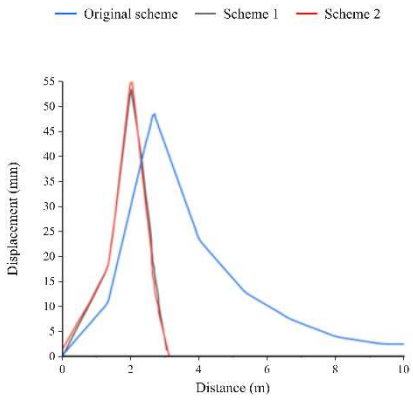
(a) Horizontal Displacement Nephogram of Roadway under the Original Scheme



(b) Horizontal Displacement Nephogram of Roadway under the Optimization Scheme 1



(c) Horizontal Displacement Nephogram of Roadway under the Optimization Scheme 2



(d) Horizontal Displacement Curve

Figure 21 Horizontal Displacement Distribution Contour

According to theoretical calculations and numerical simulations, combined with the support experience and application performance of the excavated track blind inclined shaft and upper section of the return air blind inclined shaft, the optimized scheme reduces support boreholes and support density, while its control effects on surrounding rock deformation, stress and plastic zone are basically equivalent to those of the original scheme, fully meeting the long-term stability requirements of deep large-inclination roadways. The support form of "bolt-mesh-shotcrete + cable" is adopted for the roadway section of the lower section of the return air blind inclined shaft, and Optimization Scheme 2 is applied for support.

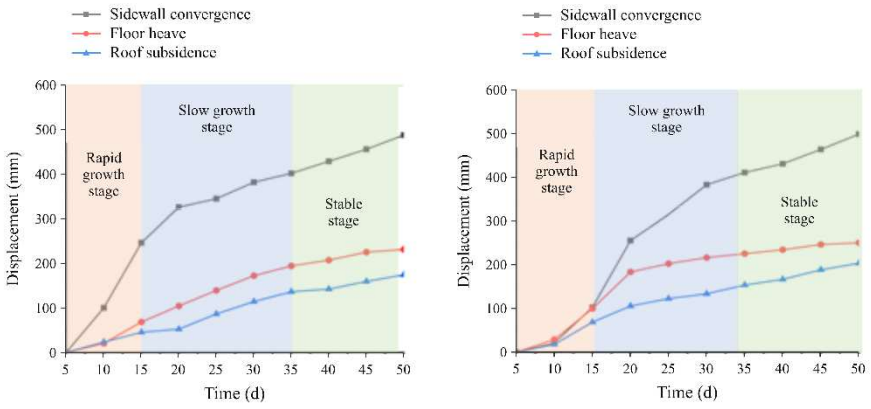
Seven anchor cables are arranged in each row on the full-section arch of the roadway, including

three 8.3 m-long cables and four 4.3 m-long cables. The cable body is 1 × 19 strand steel strand with a diameter of 21.8 mm and a borehole diameter of 30 mm. The hole depth for the 8.3 m-long cables is 8000 mm, and the hole depth for the 4.3 m-long cables is 4000 mm. The side cables are installed at an angle of 10° to the horizontal plane. The bolts are made of left-handed non-longitudinal rib threaded steel with a diameter of 22 mm and a length of 2400 mm. The borehole diameter is 30 mm and the hole depth ranges from 2300 mm to 2350 mm. Thirteen bolts are arranged in each row. The distance between the floor-corner side bolt and the adjacent bolt is 600 mm. The floor-corner side bolt inclines downward at 10° to the horizontal plane, and the remaining bolts are perpendicular to the roadway profile surface. The total drilling depth per excavation cycle of the optimized scheme is 92 m, while that of the original scheme is 120 m, accounting for 76.6% of the original value. The remarkable reduction in drilling workload directly cuts the drilling time for support operations and helps shorten the excavation cycle. Meanwhile, it reduces the consumption of bolt and cable materials as well as construction cost, realizing the coordinated optimization of surrounding rock control effect and excavation efficiency. In addition, by adopting high-strength bolt and cable materials and optimizing spacing, row spacing and installation angles, the long-term stability of surrounding rock can still be guaranteed under reduced support density.

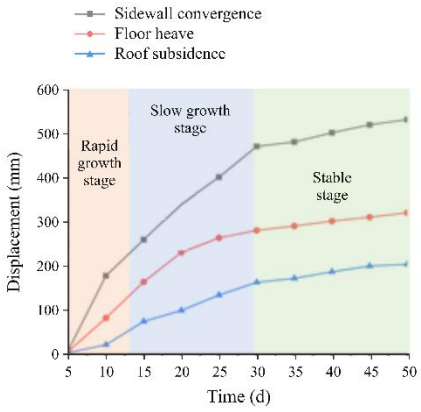
4.4 Field Monitoring Results

To systematically verify the comprehensive support performance, a 100 m test section was established from K0+150 m to K0 + 250 m in the lower section of the return air blind inclined shaft. The full optimized scheme was implemented and its performance was recorded strictly. The construction data of the original scheme from the section before the application of the optimized scheme were selected for comparison.

To verify the optimized permanent support scheme, the deformations of roof, floor and two sidewalls at three cross-sections were monitored for 50 days. The monitoring data are shown in Table 4.



(a) Monitoring Section I (b) Monitoring Section II



(c) Monitoring Section III

Figure 22 Variation Diagram of Surface Displacement of Rock Roadway

Table 4 Maximum Displacement of Surrounding Rock in the Section

Monitoring Section	Maximum Roof Subsidence / mm	Maximum Floor Heave / mm	Maximum Sidewall Convergence / mm
Section I	180	224	498
Section II	201	261	500
Section III	208	317	513

Monitoring results indicate that under the optimized permanent support scheme, roof displacement at the excavation face exhibits an evolutionary characteristic of initial deformation release followed by gradual convergence, and finally stabilizes at approximately 205mm, complying with safety regulatory requirements. Although the sidewall convergence and floor heave are more significant than roof deformation, their measured extreme values are in a safely controlled state and do not exceed the safety threshold. It can be concluded that after adopting this support scheme, the surrounding rock condition at the excavation face is favorable, ensuring the normal service of the roadway.

5 Conclusions

(1) This study reveals that the failure mechanism of anchor cables in deep large-inclination roadways undergoes a fundamental transition, shifting from conventional tension-dominated failure to shear-dominated tension-bending-shear composite failure. The traditional support design method that only considers axial tension has serious limitations and cannot effectively assess actual risks, which consequently leads to support failure. Accordingly, the core principle for support optimization requires innovation. The key measure is to adopt a strategy of installing bolts and cables perpendicular to rock strata with high pre-stress, so as to fundamentally restrain surrounding-rock deformation and mitigate shear loads and achieve a safe and reliable support system.

(2) The study finds that the displacement, stress and plastic zone range of roadway surrounding rock all reach peak values at a dip angle of 5°. This demonstrates that small dip angles induce the most severe disturbance to surrounding-rock equilibrium, representing the most unfavorable condition that requires close attention in practical engineering. When the dip angle exceeds 15°, especially in the range of 20°~25°, stable asymmetric bearing structures are formed inside the surrounding rock, which successfully transfer vertical loads, resulting in a significant reduction of vertical stress and decreased deformation tending to stability.

(3) For the roadway with a dip angle of 17° where stable structures have been formed, the optimized scheme reduces the number of bolts from 15 to 13 and enlarges bolt spacing and row spacing. By adopting high-strength 1×19-strand anchor cables, optimizing support spacing and row spacing, and shortening part of the long anchor cables, the drilling workload for support is reduced by 23.3%. Joint verification by numerical simulation and field monitoring shows that the stability indexes of the optimized roadway are basically equivalent to those of the original scheme, which verifies the rationality and effectiveness of this principle. On the premise of ensuring safety, remarkable savings in support materials and improvement in construction efficiency are achieved, providing successful cases and theoretical basis for cost reduction and efficiency improvement in deep mines.

Funding:

No funding was received for this study.

Data availability：

The data supporting the findings of this study are not publicly available due to confidentiality restrictions imposed by the participating mine. Access may be granted through the corresponding author upon reasonable request and with permission from the mine.

References

1. Zang, C.; Chen, M.; Zhang, G.; Wang, K.; Gu, D. Research on the failure process and stability control technology in a deep roadway: Numerical simulation and field test. *Energy Sci. Eng.* **2020**, *8*, 2297–2310. [CrossRef]
2. Liu, S.; Bai, J.; Wang, X.; Yan, S.; Zhao, J. Field and numerical study on deformation and failure characteristics of deep high-stress main roadway in Dongpang Coal Mine. *Sustainability* **2021**, *13*, 8507. [CrossRef]
3. Wu, C.; Qin, T.; Wang, L.; Liu, Z. Research on surrounding rock control technology of Dongbaowei deep mining roadway. *Adv. Civ. Eng.* **2021**, *2021*, 6660989. [CrossRef]
4. Liu, S.; Liu, H.; Xie, K.; Shan, L.; Xiao, F.; Wang, B.; Wang, Y. Stability analysis and support optimization for a coal mine roadway subjected to high horizontal stress. *Appl. Sci.* **2025**, *15*, 2276. [CrossRef]
5. Li, D.; Gong, H.; Han, Z.; Ru, W.; Luo, P. Characteristics of mining-induced stress rotation due to unloading in deep roadway excavation and surrounding rock control countermeasures. *Appl. Sci.* **2025**, *15*, 9950. [CrossRef]
6. Xiong, X.; Nie, W.; Ouyang, Y.; Dai, J.; Huang, Y. Principal stress rotation effect and multi-factor coupling support optimization in roadways of inclined coal seams. *Sci. Rep.* **2025**, *15*, 25628. [CrossRef]

7. Shan, R.; Bai, H.; Wang, H.; Wu, H.; Sun, P.; Nie, M.; Li, Y.; Xiao, S.; Liu, D. Deformation and failure mechanisms of roadway surrounding rock in inclined stratified rock masses. *Eng. Fail. Anal.* **2025**, *182*, 110083. [CrossRef]
8. Qi, X.; Wang, R.; Mi, W. Failure characteristics and control technology of surrounding rock in deep coal seam roadway with large dip angle under the influence of weak structural plane. *Adv. Civ. Eng.* **2020**, *2020*, 6623159. [CrossRef]
9. Liu, H.; Xu, C.; Wang, H.; Li, G.; Fan, S. Investigation on surrounding rock stability control technology of high stress roadway in steeply dipping coal seam. *Adv. Civ. Eng.* **2021**, *2021*, 5269716. [CrossRef]
10. Wu, H.; Jia, Q.; Wang, W.; Zhang, N.; Zhao, Y. Experimental test on nonuniform deformation in the tilted strata of a deep coal mine. *Sustainability* **2021**, *13*, 13280. [CrossRef]
11. Fang, W.; Li, M.; Huang, P.; Shi, T.; Chen, Y.; Ma, S.; Ren, G. Study on failure mechanism and control of surrounding rock of inclined strata crossing roadway in deep coal mine. *Front. Earth Sci.* **2024**, *12*, 1338670. [CrossRef]
12. Sun, G.; Liu, L.; Ao, Y.; Hu, Y.; Wang, S.; Kang, X.; Liu, Y. Composition characteristics of soft coal seams with large inclination angles and mining heights and the deformation of roadway surrounding rocks. *Sci. Rep.* **2025**, *15*, 43152. [CrossRef]
13. Li, F.; Zhang, B.; Guo, J.; Li, Z.; Xie, Y.; Xu, Q.; Duan, D. Cross-section shape and asymmetric support technology of steeply inclined thick coal seam roadway. *Appl. Sci.* **2025**, *15*, 5976. [CrossRef]
14. Liu, J.; Dang, Y.; Ji, C. The regularity of asymmetric evolution of stress and displacement fields in surrounding rock during horizontal stratified mining of steeply inclined, extra-thick coal seams. *Front. Mater.* **2026**, *13*, 1771605. [CrossRef]
15. Wu, G.; Jia, S.; Chen, W.; Yuan, J.; Yu, H.; Zhao, W. An anchorage experimental study on supporting a roadway in steeply inclined geological formations. *Tunn. Undergr. Space Technol.* **2018**, *82*, 125–134. [CrossRef]
16. Li, A.; Dai, F.; Wu, W.; Liu, Y.; Liu, K.; Wang, K. Deformation characteristics of sidewall and anchorage mechanisms of prestressed cables in layered rock strata dipping steeply into the inner space of underground powerhouse cavern. *Int. J. Rock Mech. Min. Sci.* **2022**, *159*, 105234. [CrossRef]
17. He, M.; Ren, S.; Guo, L.; Lin, W.; Zhang, T.; Tao, Z. Experimental study on influence of host rock strength on shear performance of Micro-NPR steel bolted rock joints. *Int. J. Rock Mech. Min. Sci.* **2022**, *159*, 105236. [CrossRef]
18. Rong, H.; Pan, L.; Li, X.; Wang, M.; Qu, Z.; Lu, M.; Guo, K. Analysis on influence factors of roadway instability in high-stress, steeply inclined extra-thick coal seam. *Adv. Civ. Eng.* **2021**, *2021*, 4676685. [CrossRef]
19. Guo, K.; Ji, M.; Liu, Y.; Wang, Q.; Guo, Z.; Peng, J. Study on the load-bearing mechanism of tensile prestressed bolt–cable coupled support in deep roadways. *Appl. Sci.* **2025**, *15*, 12418. [CrossRef]
20. Qiang, X.; Li, J.; Chen, C.; Dong, J.; Zheng, Y.; Chen, Z. Nonuniform deformation instability mechanism of gob-side entry retained in inclined coal seam and stability control. *Appl. Sci.* **2023**, *13*, 8727. [CrossRef]
21. Wang, B.; Zhou, D.; Zhang, J. Research on deformation characteristics and control technology of surrounding rock for gob-side entry with small coal pillar in gently inclined coal seam. *Energy Sci. Eng.* **2024**, *12*, 1759–1774. [CrossRef]

22. Xie, Z.; Wang, J.; Zhang, N.; Guo, F.; He, Z.; Xiang, Z.; Zhang, C. Study on time-dependent failure mechanisms and CBAG differential support technology of roadway in steeply inclined coal seam. *Processes* **2023**, *11*, 866. [CrossRef]
23. Zhang, S.; Ren, C.; Gao, X.; Gao, Y.; Nie, L.; Li, S.; Jiang, M. Stability and control of surrounding rock of a trapezoidal roadway retained with hard roof cutting. *Appl. Sci.* **2025**, *15*, 348. [CrossRef]
24. Tian, Z.; Ma, L.; Liu, Y.; Xiao, Z.; Zhang, Y.; Li, S. Multi-scale modeling and sensitivity analysis for weak roadway areas: A case study of Xiaoyun coal mine. *Sci. Rep.* **2026**, *16*, 11658. [CrossRef]
25. Wang, Z.; Dou, L.; Wang, G. Coal burst induced by horizontal section mining of a steeply inclined, extra-thick coal seam and its prevention: A case study from Yaojie No. 3 Coal Mine, China. *Shock Vib.* **2019**, *2019*, 8469019. [CrossRef]
26. Wang, Z.; Dou, L.; Wang, G.; He, J.; Hu, J. Failure mechanism of anchored roadway surrounding rocks under near-field dynamic disturbance. *KSCE J. Civ. Eng.* **2024**, *28*, 2454–2468. [CrossRef]
27. Wang, E.; Yin, S.; Kang, Q.; Zhao, X.; Lan, Q.; Sheng, H.; Liang, H. Coupling control technology of anchoring and unloading in deep intense-mining and large-deformation roadway: A case study. *Sci. Rep.* **2024**, *14*, 12075. [CrossRef]
28. Han, G.; Dou, L.-M.; Xie, J.-H.; Zhao, Q.; Shao, Y.-W.; Sun, M.-M.; Mou, L. Research and engineering practice of coupled unloading and supporting technology for rock burst prevention in hard coal seams of the Ordos region. *Front. Earth Sci.* **2025**, *13*, 1712323. [CrossRef]
29. Lu, S.; Sun, M.; Niu, S.; Zhang, Y. Variation characteristics of support strength and stability in post-peak large deformation for roadways surrounding rock. *Sci. Rep.* **2025**, *15*, 41642. [CrossRef]
30. Ge, X.; Wang, L.; Yang, K.; Wu, M. A modified Unlu–Gercek longitudinal deformation profile for circular inclined roadway: Incorporating spatial and geomechanical parameters. *Appl. Sci.* **2026**, *16*, 7619. [CrossRef]